ADVANCED FUNCTIONAL MATERIALS
www.afm-journal.de

An Oral Nanovaccine Secreted by Genetically Engineered and Ultrasound-Responsive Bacteria for Colon Cancer Immunotherapy

*Jiexin Li, Ruiqi Yang, Yihang Yuan, He Ren, Chao Fang, Jonathan F Lovell, and Yumiao Zhang**

Colorectal cancers represent a major global morbidity and mortality burden, neccessitating improved treatment paradigms. In this work, an ingestible, genetically engineered *Escherichia coli* (*E. coli*) 1917 termed "*E. coli* (AH1-CDA-Co1)" is designed that upon ultrasound exposure secretes bacterial outer membrane vesicles (OMV) incorporating the AH1 tumor rejection epitope, an enzyme producing the stimulator of interferon genes (STING) agonist CDA, and the microfold cell-targeting peptide Co1. For oral administration, a polydopamine system (iPDA) coating on bacteria is exploited to resist the acidic condition in stomach, increase the bacterial survival, and prolong the intestinal transit time. Upon harmless ultrasound exposure, sustained secretion of engineered OMV vaccines is triggered that efficiently cross the intestinal epithelium. Both cyclic GMP–AMP synthase (cGAS)-STING and TLR4 innate immune signaling pathways are activated, triggering long-term antigen-specific immune responses that overcome the immunosuppressive tumor microenvironment. In subcutaneous and orthotopic murine colorectal tumor models, the *E. coli* (AH1-CDA-Co1)@iPDA system inhibits tumor growth and prolongs survival without recurrence. *E. coli* (AH1-CDA-Co1)@iPDA also inhibits tumor growth and recurrence in a postoperative orthotopic colonrectal tumor model of lymph node metastases. Taken together, *E. coli* (AH1-CDA-Co1)@iPDA demonstrates a potent oral vaccine system for improved colon cancer immunotherapy.

1. Introduction

Colon cancer is responsible for nearly one million deaths per year worldwide, with a case incidence predicted to increase by 50% in 20 years.[1] As such, the development of new therapeutic approaches is greatly needed. Oral vaccines have great potential for treating colon cancer as the intestine represents the largest mucosal immunologic system. However, the harsh gastrointestinal (GI) environment and the intestinal epithelial permeability barrier seriously hinder the development of effective oral vaccines.[2] To overcome the intestinal epithelial barrier, natural properties of microorganisms was exploited for the development of oral poliovirus vaccines that have also entered clinical trials.[3] Also, in order to enhance the intestinal epithelial barrier, various microfold (M)-cell targeted moieties were designed to be included in oral nanovaccines.[4] Other recent advances on oral vaccines include the first FDA-approved oral immunotherapy drug for alleviation peanut allergic reactions, named Palforzia that could effective stimulate mucosal immunity.[5] In addition, given the abundant presence of microbiota in the intestine, oral engineered commensal microorganisms were proposed as a potent platform to elicit mucosal immune responses for oral immunotherapy.[6] Therefore, an ideal oral vaccine with sustained immune responses should meet the following requirements including tolerance to the acidic environment of the gastrointestinal tract, long enough residence time in GI tract, permeability to pass intestinal epithelial barrier.

Among the biomaterials used as oral vaccines, outer membrane vesicles (OMVs) have attracted research attention for oral immunotherapy due to their good intrinsic immunostimulatory properties and capability of penetrating intestinal epithelial barrier for subsequent direct interaction with immune cell in the lamina propria.[7] The OMVs can also be used as a scaffold or carrier to deliver antigens for further induction of synergistic antitumor immune responses.[8] However, OMVs themselves cannot resist the harsh gastrointestinal environment in GI tract, so direct oral administration of OMVs is not a viable route for

J. Li, R. Yang, H. Ren, Y. Zhang
School of Chemical Engineering and Technology
Key Laboratory of Systems Bioengineering (Ministry of Education)
Frontiers Science Center for Synthetic Biology (Ministry of Education)
Tianjin University
Tianjin 300350, P. R. China
E-mail: ymzhang88@tju.edu.cn
Y. Yuan, C. Fang
Hongqiao International Institute of Medicine
Tongren Hospital and State Key Laboratory of Systems Medicine for Cancer
Department of Pharmacology and Chemical Biology
Shanghai Jiao Tong University School of Medicine
Shanghai 200025, China
J. F Lovell
Department of Biomedical Engineering
The State University of New York at Buffalo
Buffalo, NY 14260, USA

The ORCID identification number(s) for the author(s) of this article can be found under https://doi.org/10.1002/adfm.202414994

DOI: 10.1002/adfm.202414994

oral immunotherapy. Genetically engineered bacteria, with arabinose as the gene expression inducer were made and the derived OMVs containing tumor antigens were used as an oral vaccine that could penetrate the intestinal epithelium into the lamina propria to activate immune responses,[2a] but chemical inducers cannot regulate desired gene expression in specific diseased sites.[9] In particular, given the snaked structure of the intestine deeply seated under layers of fat in the abdomen, overcoming the penetration depth issue is important for colon cancer therapy if precise spatiotemporal secretion of OMVs and stimulation of immune responses by external stimuli are preferred.

Ultrasound (US) as a good stimulus with the advantages of deep penetration, high safety profile, and noninvasiveness has been widely used for tumor diagnosis and treatment.[10] Some application examples include diagnostic imaging,[11] sonodynamic therapy,[12] immunotherapy,[13] and local drug activation.[14] For example, taking advantage of US, gas vesicles generated from microorganisms were used to visualize bacterial gene expression in vivo.[15] US as an external stimulus, is easier to be controlled to regulate bacterial gene expression in desired site to achieve local drug release.[13,16] In addition, compared with the commonly used bacterial gene expression inducers including chemical, physical stimulation and biological approaches,[9a,17] US has many advantages in terms of deep penetration capability and flexible controllability. US can precisely regulate bacterial gene expression and drug release in living animals in a spatiotemporally controllable manner to avoid unwanted adverse toxicity.[18] However, the potential use of US as an inducer for gene expression in orally administered bacteria as colon cancer vaccines has not yet been explored.

To address the challenges associated with limited spatiotemporal controllability and poor immune response activation in GI tract, herein, we developed an ultrasound-controllable genetically engineered bacteria as an in situ oral tumor vaccine, which was termed *E. coli* (AH1-CDA-Co1)@iPDA, for the treatment of colon cancers (**Figure 1**). The plasmid simultaneously encoding the antigen AH1, adjuvant CDA, and targeting peptide Co1 gene was designed, which was then used to transform *E. coli* 1917. After spatiotemporal ultrasound irradiation, the engineered bacteria were activated to secrete OMVs containing antigens, adjuvants, and M cell-targeting peptides as in situ oral vaccines for colon cancer tratment. In addition, polydopamine encapsulation and gastrointestinal synthetic epithelial lining (iPDA) system were used to enable the engineered bacteria resist to the gastrointestinal environment and prolong the transit time of bacteria for enhanced immunity. Long-term antigen-specific immune memory responses and alleviation of the immunosuppressive tumor microenvironment were achieved as demonstrated in multiple murine cancer models, showing the potential preclinical and clinical use of the *E. coli* (AH1-CDA-Co1)@iPDA nanoplatform for cancer treatment.

2. Results and Discussion

2.1. Construction of Ultrasound-Responsive Plasmid and Genetically Engineered Bacteria

An US-controllable plasmid encoding genes of antigen and adjuvant was desgined for oral cancer vaccines. To fluorescently investigate the process, a surrogate model plasmid encoding ClyA-mCherry inClyA-MYC-AH1-CDA-Co1 was first designed using pR-pL tandem promoter (**Figure 2A**). The recombinant plasmid was subsequently transformed into *E. coli* 1917 to yield target peptide-containing OMVs. As shown in Figure 2B and Figure S1 (Supporting Information), upon US irradiation, the increase of mCherry fluorescence was evidently observed in OMVs, indicating the US-mediated expression of mCherry.

Next, the mechanism of US activation of gene expression was investigated. Therefore, mCherry expression was also studied at different temperatures. As shown in Figure 2C, after incubation at 37 °C, OMVs showed no fluorescence signal, indicative of minimal expression of ClyA-mCherry. In contrast, after temperature for the bacterial culture was raised to 43 °C, strong red fluorescence signals could be detected in OMVs. The fluorescence signal of OMVs kept increasing when bacteria was incubated at 43 °C from 30 to 60 min, suggesting that the US-regulated expression of target protein in genetically engineered bacteria was realized by its thermo-sensitivity (Figure 2D). Transmission electron microscopy (TEM) demonstrated that OMVs had uniform sphere morphology with the double lipid-layers structures (Figure S2, Supporting Information). Parameters of ultrasound such as irradiation duration and different powers were optimized and we found that irradiation at 4 W for 6 min could keep the bacterial solution at 43 °C (Figure S3, Supporting Information). In addition, US and heat treatment had no obvious side effect on the growth of the engineered bacteria (Figure 2D; Figure S4, Supporting Information). The suitability of use of US to spatiotemporal regulate the gene expression in vivo was also investigated. As shown in Figure S5A (Supporting Information), the temperature in the irradiated tissue of the mouse could increase to 43 °C by optimized US power parameters (4 W). Strong fluorescent signals of mCherry were also clearly observed in the intestines of mice excised after gavage of genetically engineered bacteria with US irradiation, but not in other control groups (Figure 2F,G; Figure S5B, Supporting Information).

2.2. OMVs Are Able to Penetrate the Intestinal Epithelial Barriers

Penetration of the epithelial barrier and delivery to PPs via M cells are key steps to initiate mucosal immune responses for oral immunotherapy.[19] Therefore, to enhance the activation of intestinal mucosal immune responses, target gene of ClyA-MYC-AH1-CDA-Co1 was designed by fusing M cell targeting peptide Co1 (SFHQLPARSPLP)[20] to the C-terminus of the surface protein ClyA of OMVs. AH1 antigen peptide (SPSYVYHQF), agonist CDA-producing enzymes (diadenylate cyclase) were encoded in plasmid. In particular, diadenylate cyclase was used to catalyze two molecules of ATP or ADP to yield c-di-AMP (CDA). Two characteristic structures including DGA and RHR in the DAC domain are conserved in almost all proteins with DAC domains, which plays a key role in this catalytic process.[21] Also, controls such as *E. coli* (AH1), *E. coli* (AH1-CDA) with MYC tags were also designed (Figure 2A). The OMVs secreted by these strains induced by US were denoted as OMV (AH1), OMV (AH1-CDA) and OMV (AH1-CDA-Co1). To highlight the effect of US, control OMVs without US induction were also prepared and labelled as OMV (AH1-CDA-Co1) (-US) ("-US" was used to denote no

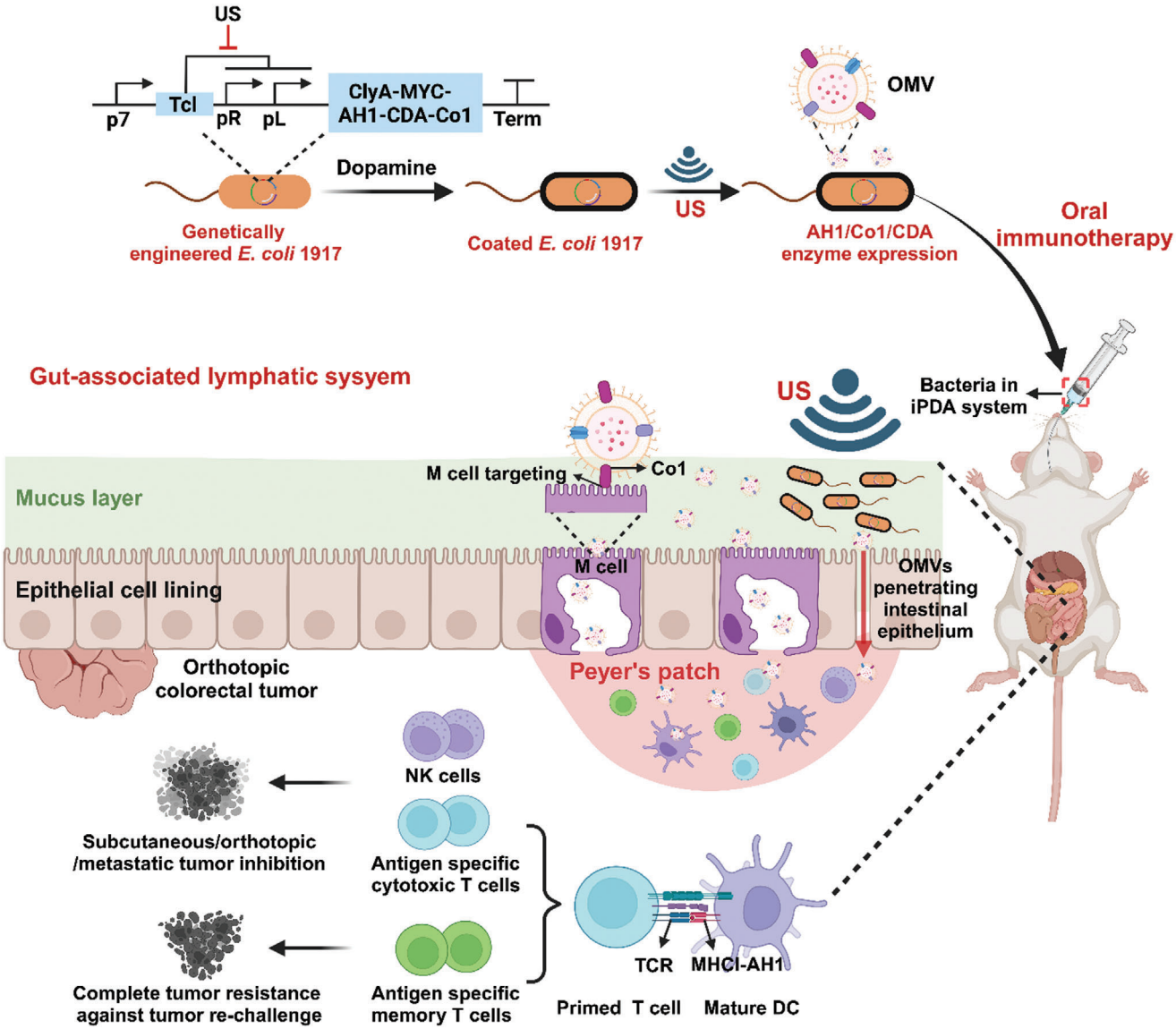

Figure 1. Design, preparation, and mechanism of *E. coli* (AH1-CDA-Co1)@iPDA as an in situ ultrasound-responsive oral vaccine for colon cancer treatment. Construction of ultrasound-responsive and genetically engineered bacteria secreting OMVs as tumor vaccines. OMVs tumor vaccines target PPs to activate the gut-associated lymphatic immune system. After oral administration of engineered *E. coli*, OMV (AH1-CDA-Co1) carrying tumor antigens, adjuvants and targeting peptides was sustainably generated in intestines after ultrasound irradiation. Owing to the M cell-targeting effect of Co1, OMV (AH1-CDA-Co1) effectively penetrated the intestinal epithelial barrier and reached PPs to activate antigen-specific mucosal immunity for color tumor inhibition. Created with BioRender.com.

US irradiation throughout the text since no target genes would be expressed in this scenario). The expression of MYC-tag in OMVs was verified by western blot under US or 43 °C control (Figure 2H), indicating that the expression of the target gene remained deactivated at 37 °C, but became activated when induction by 43 °C and US. TEM showed that all OMVs exhibited a bilayer structure and uniform particle size distribution (Figure 2I; Figure S6A,B, Supporting Information).

To verify that OMVs produced in situ can enter PPs through M cells, we evaluated the efficiency of OMV uptake by M cells in vitro and in vivo. Caco-2 cells were cultured in the upper chamber of a transwell system for 14 days to allow the differentiation of M cells.[22] After adding the 1,1-dioctadecyl-3,3,3,3-tetramethylindotricarbocyanine iodide (DiO) labeled OMVs derived from different engineered bacteria to the upper chamber, the fluorescence intensity in the lower culture medium was detected (Figure S7, Supporting Information). As shown in Figure 2J, the uptake efficiency of OMVs containing Co1 targeting peptide (OMV (AH1-CDA-Co1)) was ≈2 times more than that of other OMVs. Surprisingly, the ability of OMVs to cross the intestinal epithelium was slightly enhanced by US irradiation (Figure 2J). This may be because the intestinal epithelium becomes more permeable for the penetration of OMVs after US exposure.[23] Next, we assessed the penetration ability and PPs

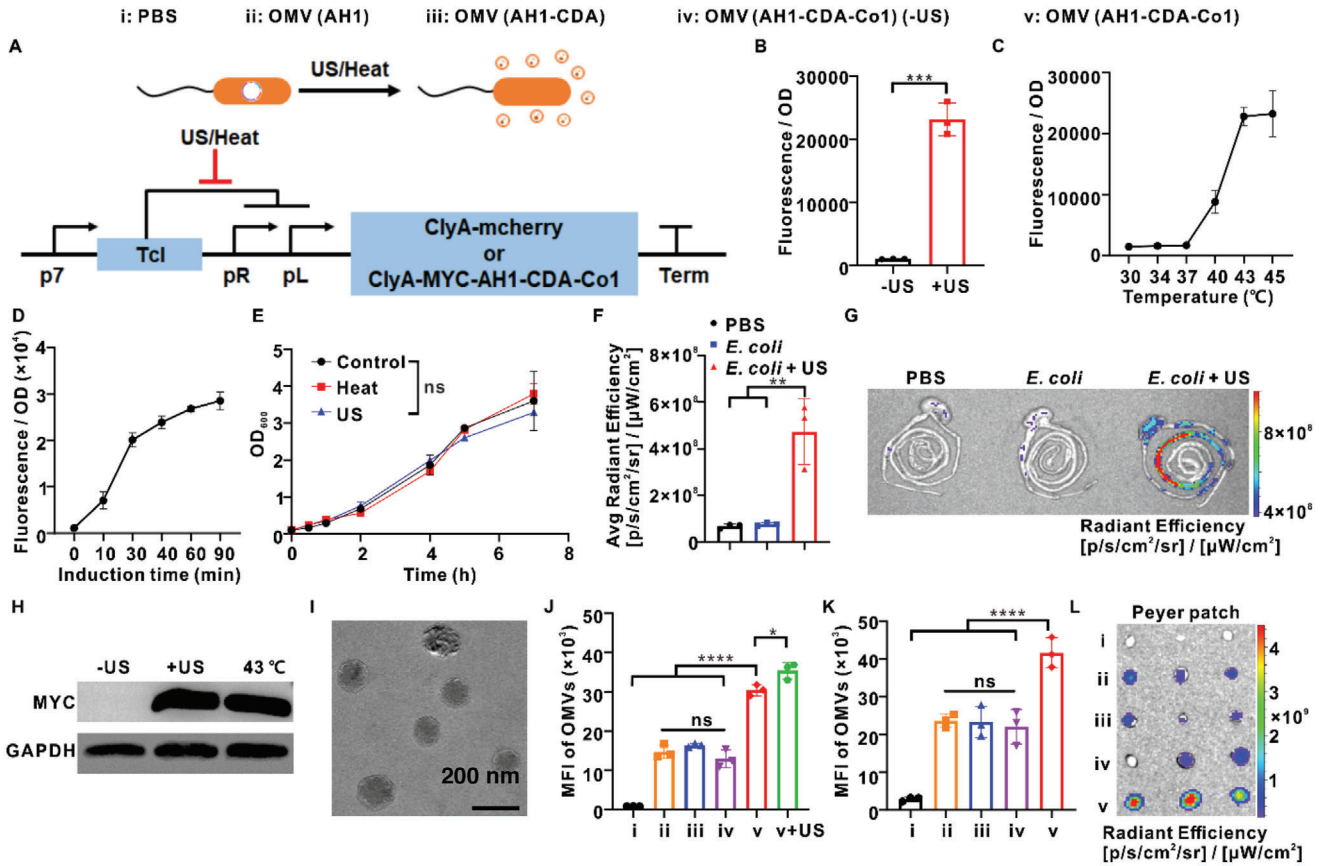

Figure 2. Outer membrane vesicles (OMVs) containing AH1 and CDAs are permeable to epithelial barriers. A) Illustration of US responsive plasmid design. B) Fluorescence of mCherry protein expressed from bacteria with and without US irradiation ($n = 3$). C,D) Fluorescence of mCherry protein expressed from bacteria at different temperatures and with US irradiation. E) Growth curves of bacterial after treatment with 43 °C heating or US irradiation (4 W) for 30 min ($n = 3$). The untreated bacterial was used as the control. The number of bacteria was determined at OD_{600}. F,G) Fluorescence quantifications by mCherry and images of intestines excised from mice after oral administration of 1×10^8 CFU of bacteria with US irradiation for 6 h ($n = 3$). Images were representative of three experiments. H) Western blot of MYC nanobodies. Cells were induced for 30 min at 43 °C with or without US, then suspended in 5 mL of media for 24 h at 37 °C. I) Morphology of OMVs by TEM. Scale bar, 200 nm. J) The fluorescence of OMVs (fluorescently labeled by DiO) in the lower chamber of Transwell system after 4 h ($n = 3$). K) Analysis of epithelial penetration of OMVs (20 μg mL^{-1} protein) derived from the different indicated engineered bacterial vaccines in vitro ($n = 3$). L) Fluorescence images of OMV distribution in PPs after mice were given different indicated engineered bacterial vaccines in vivo. i: PBS, ii: OMV (AH1), iii: OMV (AH1-CDA), iv: OMV (AH1-CDA-Co1) (-US), v: OMV (AH1-CDA-Co1). Data are represented as mean ± S.D; Statistical significance was calculated via one-way ANOVA with Turkey's test: $^{ns}p > 0.05$; $^{*}p < 0.05$; $^{**}p < 0.01$; $^{***}p < 0.001$; $^{****}p < 0.0001$.

targeting ability of OMVs in vivo. Mice were first anesthetized and then the intestinal segment containing PPs was ligated. Different OMVs were subsequently injected into the ligated intestinal cavity. After incubation for 2 h, the ligated intestinal segment and PPs were collected for fluorescence quantification. As shown in Figure 2K,L, OMV (AH1), OMV (AH1-CDA), and OMV (AH1-CDA-Co1) (-US) could penetrate the intestinal epithelial barrier. However, OMV (AH1-CDA-Co1) exhibited enhanced penetration and PPs targeting ability. In addition, we studied the uptake of OMVs by M cells in PP by immunofluorescence staining. As shown in Figure S8 (Supporting Information), compared with *E. coli* (AH1-CDA)@iPDA, DiO labeled OMVs derived from *E. coli* (AH1-CDA-Co1)@iPDA were taken up more by M cells in PP with brighter green fluorescence (DiO) due to the presence of Co1.

2.3. US-Responsive OMVs Activate Antigen-Specific Immune Responses In Vitro After Epithelial Penetration

To further investigate whether OMVs can activate immune responses after passing through intestinal epithelial barriers, we used the above-mentioned transwell system and seeded Caco-2 cells and bone marrow derived dendritic cells (BMDCs) in the upper and lower chamber, respectively (Figure S9, Supporting Information). We found that OMV (AH1-CDA-Co1) were effectively taken up by BMDCs after penetrating the epithelial barrier compared with other OMVs (Figure S10, Supporting Information). In addition, compared with OMV (AH1), OMV (AH1-CDA), the addition of STING agonist could more effectively enhance the activation of the cGAS-STING pathway featuring phosphorylation of TBK1, P65 and IRF3 proteins and secretion of

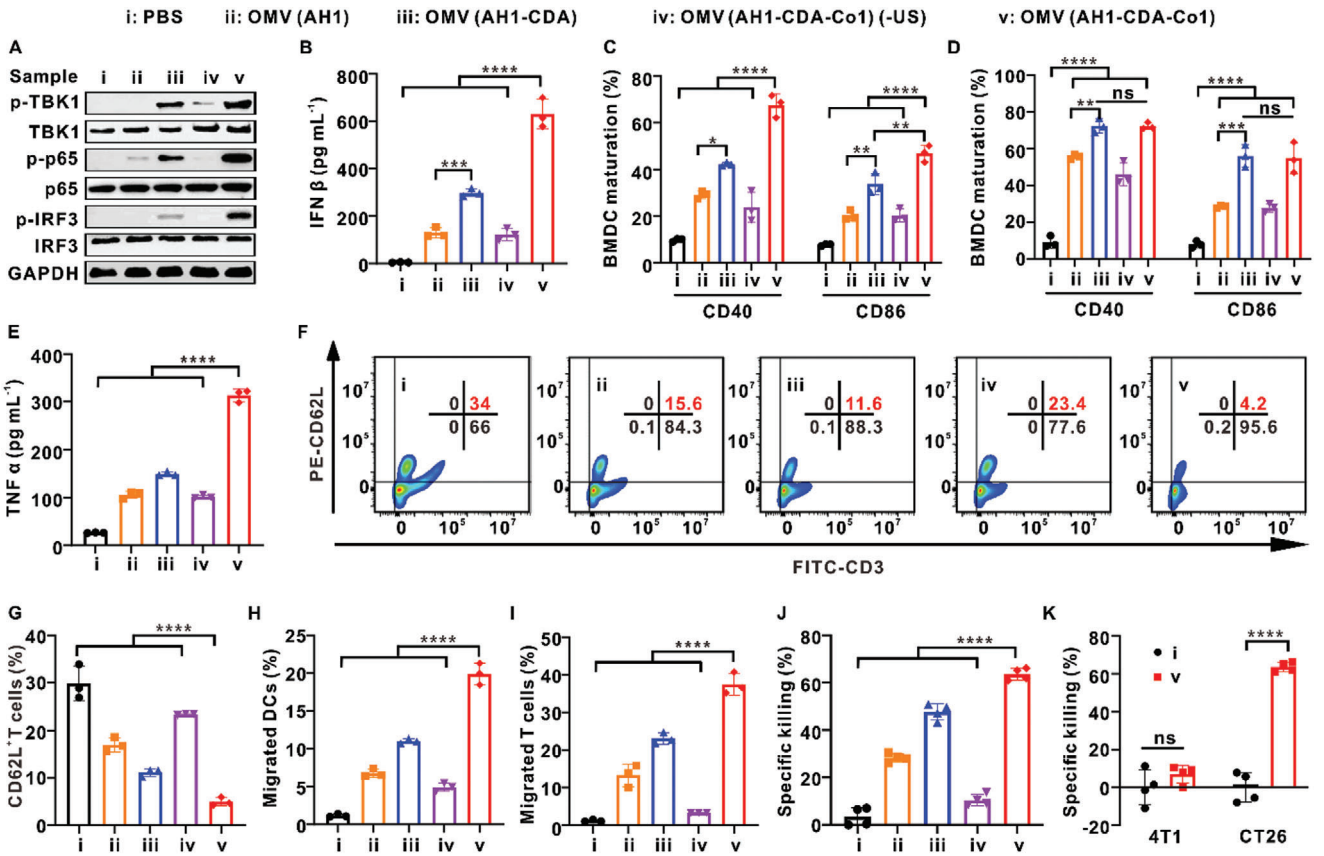

Figure 3. In vitro immune responses stimulated by OMVs. A) Western blotting analysis of TBK1, IRF3, p65 and phosphorylation of the indicated proteins from BMDCs treated with different formulations as indicated for 12 h. B) The expression level of IFN β from BMDCs treated with different formulations for 24 h ($n = 3$). C,D) BMDCs maturation evaluation C by Transwell system or directly incubation BMDCs and OMVs. E) The expression level of TNF α from BMDCs after treatment by different formulations for 24 h ($n = 3$). F,G) Flow cytometric plots of activated T cells ($CD3^+CD8^+CD62L^-$) ($n = 3$). H,I) Relative numbers of migrated BMDCs (H) and T cells (I) after different treatments (calculated by normalization to the number of BMDCs or T cells found in bottom wells in control group). The cytotoxic effects of T cells on (J) CT26 cells (with AH1 antigen) and (K) 4T1 cells without AH1 antigen using the CCK-8 assay ($n = 4$). i: PBS, ii: OMV (AH1), iii: OMV (AH1-CDA), iv: OMV (AH1-CDA-Co1) (-US), v: OMV (AH1-CDA-Co1). The 20 μg mL^{-1} protein OMVs were added. Data are represented as mean ± S.D. $n = 3$; Statistical significance was calculated via one-way ANOVA with Turkey's test: $^{ns}p > 0.05$; $^{*}p < 0.05$; $^{**}p < 0.01$; $^{***}p < 0.001$; $^{****}p < 0.0001$.

IFN β (**Figure** 3A,B). As expected, after stimulation with OMV (AH1-CDA-Co1), BMDCs showed the highest level of maturation ($CD40^+CD86^+$) (Figure 3C), likely due to Co1-mediated enhanced permeability and CDA-mediated STING activation. Therefore, when all OMVs were directly stimulated and incubated with BMDCs, OMV (AH1-CDA), and OMV (AH1-CDA-Co1) showed the same stimulatory ability, indicating that Co1 was the main reason for the stimulatory capability (Figure 3D). It was also found that OMVs as a natural immune adjuvant stimulated BMDCs maturation by activating the TLR4 pathway (Figure 3D). In addition, the increase of pro-inflammatory cytokine, TNF α secretion by mature BMDCs was also observed (Figure 3E). These results indicate that OMV (AH1-CDA-Co1) activated the innate immune signaling pathways of TLR4 and STING, leading to the expression of pro-inflammatory cytokines.

To investigate whether OMVs can stimulate the proliferation and priming of $CD8^+$ T cells, $CD8^+$ T cells isolated from the spleen of BALB/c mice were co-cultured with BMDCs that were pretreated with different samples (Figure S9, Supporting Information). After OMV (AH1-CDA-Co1) treatment, the number of mature T cells ($CD62L^-$) increased significantly (95.0%) (Figure 3F,G). Next, transwell assay was conducted to evaluate the chemotaxis of immune cells (BMDCs and $CD8^+$T cells) to tumor cells. As shown in Figure 3H,I, OMV (AH1-CDA-Co1) activated most of mature BMDCs and primed $CD8^+$ T cells that were able to migrate to tumor cells effectively. In addition, AH1-specific proliferated $CD8^+$ T cells induced a significant increase in apoptosis of CT26 cells, but not other tumor cells (4T1 cells) (Figure 3J,K). These results demonstrate that OMV (AH1-CDA-Co1) holds the potential to be effectively delivered to PPs via Co1 and then activate antigen-specific tumor-infiltrating $CD8^+$ T-cell.

2.4. US-Responsive OMV (AH1-CDA-Co1) Stimulate In Vivo Intestinal Mucosal Immunity

Although advances on oral administration of naked engineered bacteria-derived OMVs to inhibit tumor growth has been reported,[2a] the bacteria might become unstable with reduced residence time in the harsh gastrointestinal environment.[24]

Therefore, in situ formulation of polydopamine-based system, iPDA was developed to coat engineered bacteria, yielding *E. coli* (AH1-CDA-Co1)@iPDA. We examined the morphology of PDA-encapsulated *E. coli* 1917 by SEM and found that *E. coli* 1917@PDA had many PDA spheres sticking to the surface of *E. coli* 1917. In addition, the color of the bacteria turned black after PDA coating. These evidences could verify the successful coating of PDA (Figure S11, Supporting Information). Specifically, *E. coli* (AH1-CDA-Co1) was first coated by polydopamine (PDA) to resist acidic condition in stomach, which was then orally gavaged, along with dopamine and trace amount of hydrogen peroxide, to enable the formation of additional PDA bacterial coating occuring on the intestinal surface. After coating with polydopamine, engineered bacteria become to resist the harsh gastrointestinal fluid as shown in **Figure** 4A and Figure S12 (Supporting Information). To quantification and visualization of bacteria, they were fluorescently labelled by our previously reported metabolic engineering approach.[25] Specifically, fluorescently labeling was obtained by incubating bacteria with azide-modified galactose, followed by conjugation fluorescence moiety of DBCO-Cy5 on the surface of bacteria. We found that the survival rate of *E. coli* @PDA after incubation with simulated gastric fluid (SGF) for 0.5, 1, 2, and 3 h was significantly higher than that of naked *E. coli* (Figure 4A). After *E. coli* @iPDA were orally administered with the protection by the iPDA system, the residence time of *E. coli* (AH1-CDA-Co1)@iPDA in the intestine was significantly prolonged by examination of fluorescence signal of bacteria in the intestine by IVIS (Figure 4B; Figure S13A, Supporting Information). This could be at least ascribed to the adhesion of engineered bacteria to the intestine, because the extracellular dopamine monomers could be immediately oxidized to polydopamines by the released oxygen generated from the reduction of hydrogen peroxide in intestine by endogenous catalase. As such, iPDA-based coating could be formed on the inner surface of intestine to achieve bacteria adhesion to intestine.[26] Twenty four hours after oral administration of *E. coli* (AH1-CDA-Co1)@iPDA, there were still bright fluorescent signals in the ex vivo intestine, which was much longer than the average transit time in the normal small intestine (60–70 min in mice and humans)[2f,27]. This coating strategy allows the *E. coli* (AH1-CDA-Co1)@iPDA to continuously secrete OMVs tumor vaccines in situ in the intestine (Figure 4C; Figure S13B, Supporting Information).

Next, we investigated whether *E. coli* (AH1-CDA-Co1)@iPDA could effectively activate intestinal AH1-specific mucosal immune responses in the subcutaneous CT26 colon tumor model. Different engineered bacteria including *E. coli* (AH1-CDA-Co1)@iPDA, *E. coli* (AH1-CDA-Co1)@iPDA (-US), *E. coli* (AH1-CDA-Co1), *E. coli* (AH1)@iPDA, and *E. coli* (AH1-CDA)@iPDA were orally administered to mice, and then US irradiation was applied to induce secretion of OMV vaccines (Figure 4D). On day 21, immune cells from PPs were isolated to evaluate the mucosal immune activation by flow cytometry. *E. coli* (AH1-CDA-Co1)@iPDA activated the strongest immune responses due to its target capability to M cells, and the cGAS-STING pathway of immune cells in PPs was effectively activated and generated type I interferon, IFN β in the serum (Figure 4E,F). IFN β facilitates cDC1s to activate NK cells and $CD8^+$ T cells through upregulating costimulatory molecules and effectively repolarizes the myeloid cells toward the proinflammatory phenotype.[28] Compared with control groups, *E. coli* (AH1-CDA-Co1)@iPDA inducted significant increase of $CD40^+$ and $CD86^+$ DC in PPs because of adjuvant CDA, M cell targeting peptide Co1 and iPDA delivery system (Figure 4G). In addition, the *E. coli* (AH1-CDA-Co1)@iPDA group exhibited the highest activation of T cells ($CD8^+$ and $CD4^+$) and NK cells in PPs (Figure 4H–K). *E. coli* (AH1-CDA-Co1) could still activated intestinal mucosal immunity, but not as potently as *E. coli* (AH1-CDA-Co1)@iPDA, indicating that the iPDA system enabled the engineered bacteria to continuously secrete OMVs vaccine for the sustained stimulation of immune cells. Not surprisingly, the immune response activated by *E. coli* (AH1-CDA-Co1)@iPDA (-US) induction is negligible (Figure 4H–K).

To verify whether the activated $CD8^+$ T cells were antigen-specific, antigen-specific immune responses in splenocytes were next evaluated. Compared with *E. coli* (AH1)@iPDA and *E. coli* (AH1-CDA)@iPDA vaccines, *E. coli* (AH1-CDA)@iPDA elicited the highest proportion of AH1 $tetramer^+$ cells in $CD3^+CD8^+$ T cells (Figure 4H–M). Next, we used the enzyme-linked immunespot (ELISpot) to evaluate the IFN-γ secretion level of splenocytes by AH1 antigen peptide restimulation. As expected, most IFN-γ was produced by splenocytes of mice immunized with *E. coli* (AH1-CDA)@iPDA (Figure 4N). In addition, the high secretion levels of proinflammatory cytokines including TNF α and IL-12p70 suggest that *E. coli* (AH1-CDA)@iPDA could reprogram the immunosuppressive tumor microenvironment (Figure 4O,P). Altogether, these results collectively demonstrate that the *E. coli* (AH1-CDA)@iPDA vaccine could effectively elicit intestinal antigen-specific immune responses in an M-cell targeting and US-responsive manner.

2.5. Antitumor Therapeutic Effect of *E. coli* (AH1-CDA-Co1)@iPDA in a Subcutaneous Colon Tumor Model

Encouraged by the results above, we next evaluated the antitumor efficacy of *E. coli* (AH1-CDA-Co1)@iPDA in a murine subcutaneous CT26 colon cancer model. CT26 tumor cells were injected subcutaneously to mice on day -10 and then mice were orally given PBS, *E. coli* (AH1)@iPDA, *E. coli* (AH1-CDA)@iPDA, *E. coli* (AH1-CDA-Co1), *E. coli* (AH1-CDA-Co1)@iPDA(-US) or *E. coli* (AH1-CDA-Co1)@iPDA vaccine for prime vaccination on day 0, followed by two booster vaccinations on days 7 and 15 (**Figure** 5A). Tumor volumes were recorded daily until day 60. In the PBS group, tumors of all mice reached 1000 mm^3 after day 14. By contrast, *E. coli* (AH1)@iPDA, *E. coli* (AH1-CDA-Co1), and *E. coli* (AH1-CDA-Co1)@iPDA (-US) slightly inhibited tumor growth inhibition (Figure 5B–E). *E. coli* (AH1-CDA)@iPDA induced moderate tumor growth inhibition. Importantly, the *E. coli* (AH1-CDA-Co1)@iPDA vaccine showed the strongest tumor growth inhibition effect compared with other groups (Figure 5B–E). On day 39, the survival rate of mice immunized with *E. coli* (AH1-CDA-Co1)@iPDA was as high as 100%, while all mice in other groups were euthanized before day 34 when tumor volume exceeded 1000 mm^3 (Figure 5D,E). Notably, *E. coli* (AH1-CDA-Co1)@iPDA vaccination led to complete tumor regression in 60% mice (Figure 5D,E).

In addition, on day 21 after treatment, the tumors were digested into single-cell suspensions for flow cytometry analysis of immune cell infiltration. As expected, after oral administration

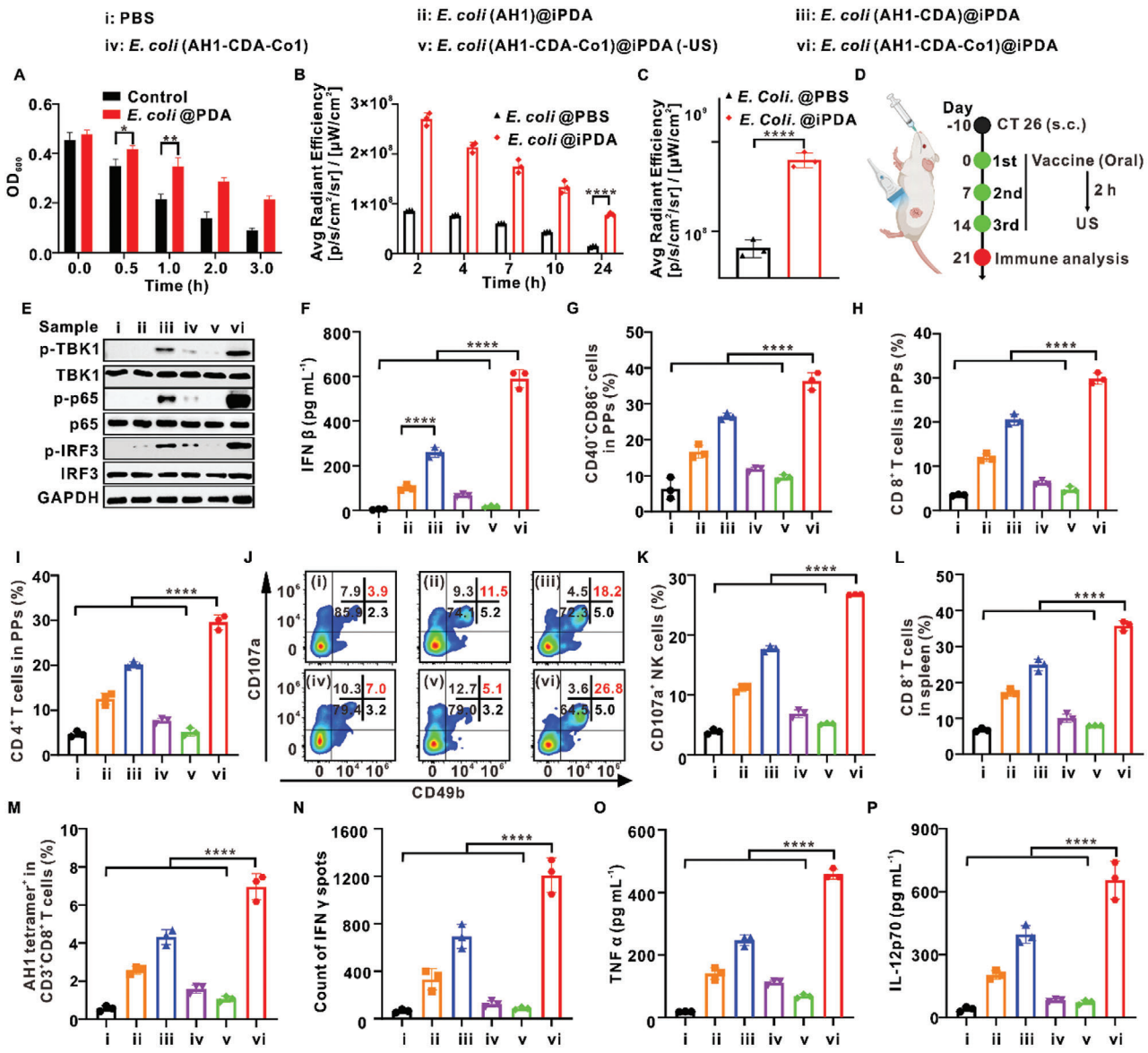

Figure 4. OMVs as oral tumor vaccines could activate sustained in vivo mucosal immune response. A) Optical density (OD) values of bacteria with or without PDA coating after incubation in simulated gastric fluid (pH 1.0, pepsin 2 mg mL^{-1}). B) Fluorescence of *E. coli*@iPDA (fluorescently labelled by Cy5) in intestine at different times. C) Fluorescence of *E. coli*@iPDA in the intestine at 24 h. D) Scheme of vaccination timeline. BALB/c mice received a subcutaneous (s.c.) injection of CT26 cells on day -10, then were immunized with the indicated oral vaccines on days 0, 7, and 14. And 2 h after gavage, the mouse abdomen was irradiated with the US for 20 min. Immune responses were analyzed on day 21. The gavage dose is 1×10^8 CFU. E) Western blotting analysis of TBK1, IRF3, p65 and phosphorylation of the indicated proteins from lymphocyte in PPs. F) IFN β cytokines were measured by ELISA after the third vaccination ($n = 3$). G–I) Quantification of mature DCs ($CD11c^+CD40^+CD86^+$) (G), $CD3^+CD8^+$ T cells (H), and $CD3^+CD4^+$ T cells (I) in PPs ($n = 3$). J,K) Representative flow cytometric plots (J) and quantification (K) of NK cell activation ($CD3^+CD49b^+CD107a^+$) in PPs ($n = 3$). L,M) Quantification of $CD3^+CD8^+$ T cells and AH1 $tetramer^+$ in $CD3^+CD8^+$ cells in spleen ($n = 3$). N) The IFN-γ secretion by splenocytes after re-stimulation with AH1 peptide was determined by the ELISpot assay ($n = 3$). O,P) Serum cytokines were measured by ELISA after the third vaccination ($n = 3$). i: PBS, ii: *E. coli* (AH1)@iPDA, iii: *E. coli* (AH1-CDA)@iPDA, iv: *E. coli* (AH1-CDA-Co1), v: *E. coli* (AH1-CDA-Co1)@iPDA (-US) and vi: *E. coli* (AH1-CDA-Co1)@iPDA. Data are represented as mean ± S.D. $n = 3$; Statistical significance was calculated via one-way ANOVA with Turkey's test: $^{ns}p > 0.05$; $^{*}p < 0.05$; $^{**}p < 0.01$; $^{***}p < 0.001$; $^{****}p < 0.0001$.

of *E. coli* (AH1-CDA-Co1)@iPDA, the infiltration of mature DCs, $CD3^+CD8^+$ T cells, and $CD3^+CD4^+$ T cells in CT26 tumor tissues all significantly increased (Figure 5F–H). In addition, *E. coli* (AH1-CDA-Co1)@iPDA immunization effectively alleviated the immunosuppressive microenvironment induced by regulatory T cells (Treg) and M2 macrophages (Figure 5I,J). These results indicate that the *E. coli* (AH1-CDA-Co1)@iPDA vaccine effectively increased the infiltration of mature DCs and T cells, as well as reduced the population of Treg cells and M2 macrophages, eventually leading to tumor growth inhibition. Also, the body weight of mice in all groups appeared normal, indicating that the engineered bacteria treatment did not cause obvious systemic

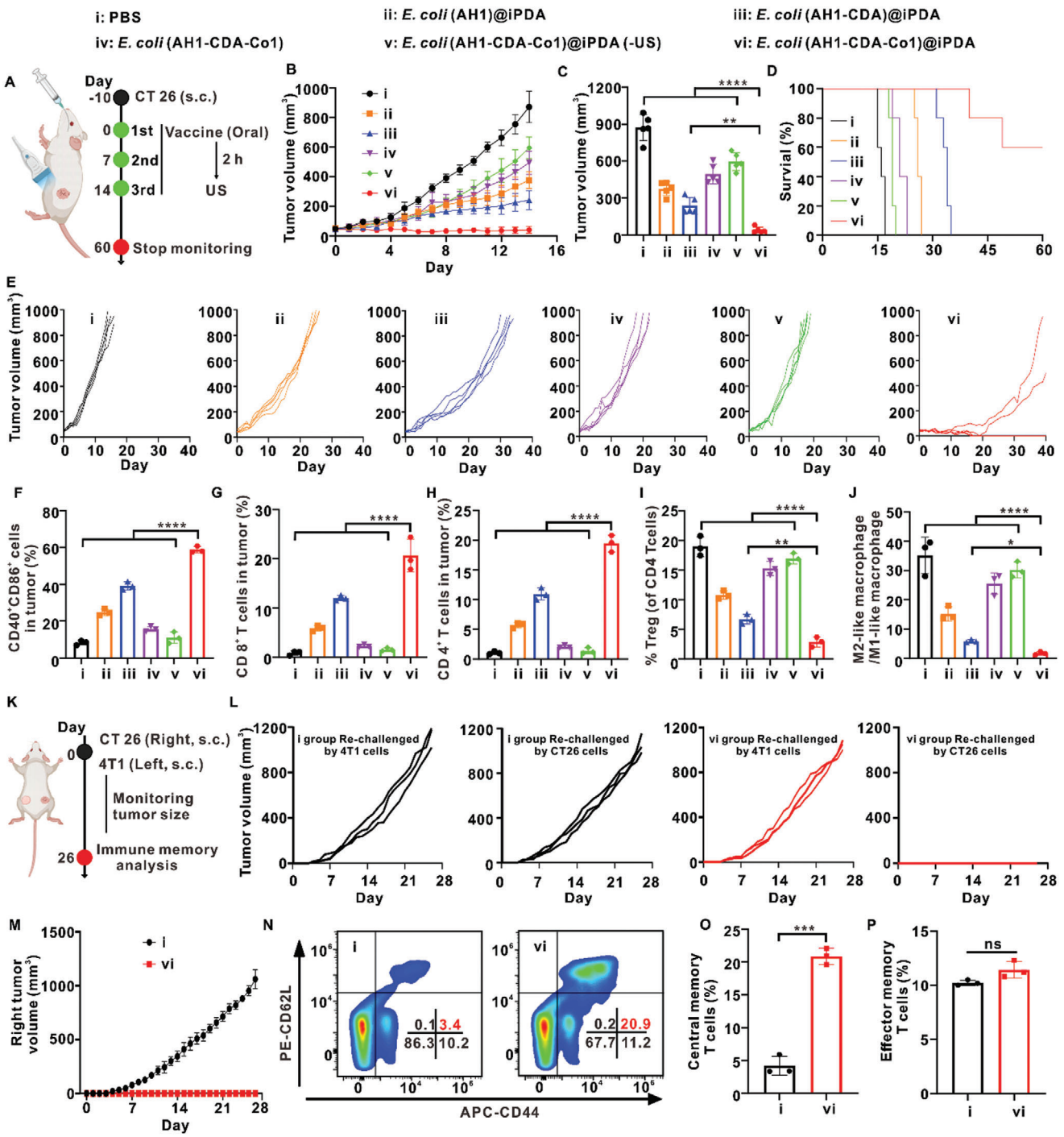

Figure 5. Antitumor efficacy and long-term immune memory by oral tumor vaccines in a subcutaneous colon cancer model. A) Scheme of timeline of model establishment and oral vaccination. BALB/c mice received subcutaneous (s.c.) injection of CT26 cells on day -10, then were immunized with the indicated oral vaccines on days 0, 7, and 14. And 2 h after gavage, the mouse abdomen was irradiated with the US for 20 min. The tumor volumes and body weight were measured every day until day 60 (data were shown as means ± S.D. from five independent mice). The gavage dose is 1×10^8 CFU. B–E) Animal survival (B–D) and tumor volumes (E) were monitored every day ($n = 5$). F–J) The infiltrating immune cells in the tumor tissues were detected by flow cytometry, including mature DC($CD11c^+CD40^+CD86^+$), $CD3^+CD8^+$ T cells, $CD3^+CD4^+$ T cells, Treg cells ($CD3^+CD4^+Foxp3^+$), M2/M1 macrophages ($F4/80^+CD206^+$/$F4/80^+CD86^+$). K) Schematic illustration of the CT26 and 4T1 tumor rechallenge experiment. $n = 3$ per group. L) Individual CT26 tumor (Right) and 4T1 tumor (Left) growth kinetics for each group. M) Average CT26 tumor cell growth kinetics. N) Immune memory investigation on day 60 by using flow cytometry by analysis of O) TCM cells ($CD3^+CD8^+CD44^+CD62L^+$) and P) the proportions of effector memory T cells ($CD3^+CD8^+CD44^+CD62L^-$) in the splenocytes ($n = 3$). i: PBS, ii: *E. coli* (AH1)@iPDA, iii: *E. coli* (AH1-CDA)@iPDA, iv: *E. coli* (AH1-CDA-Co1), v: *E. coli* (AH1-CDA-Co1)@iPDA (-US) and vi: *E. coli* (AH1-CDA-Co1)@iPDA. Data are represented as mean ± S.D. Statistical significance was calculated via one-way ANOVA with Turkey's test: $^{ns}p > 0.05$; $^{*}p < 0.05$; $^{**}p < 0.01$; $^{***}p < 0.001$; $^{****}p < 0.0001$.

toxicity (Figure S14A, Supporting Information). To further investigate whether tumor growth inhibition was ascribed to enhanced intra-tumoral immune infiltration such as tumor-infiltrating $CD8^+$ T cells, mice were treated by anti-CD8α neutralizing antibodies before treatment with *E. coli* (AH1-CDA-Co1)@iPDA to deplete $CD8^+$ T cells. By doing so, the antitumor efficiency of *E. coli* (AH1-CDA-Co1)@iPDA was significantly reduced, indicating that the important role of tumor-infiltrating $CD8^+$ T cells for inhibiting tumor growth (Figure S15, Supporting Information). In addition, the hematoxylin and eosin (H&E) of major organs such as the heart, liver, spleen, lung, and kidney and the complete blood count analysis after mice were orally given engineered bacteria showed no obvious toxicity, indicating that oral engineered bacteria have good biocompatibility (Figures S16 and S17, Supporting Information).

2.6. Long-Term Immune Memory of *E. coli* (AH1-CDA-Co1)@iPDA

To further investigate long-term immune memory, mice cured in the subcutaneous tumor model were subjected to tumor re-challenge test on day 61. 4T1 cells and CT26 cells were inoculated on the left and right flanks of mice, respectively. The tumor size was then measured every day (Figure 5K). Mice cured by *E. coli* (AH1-CDA-Co1)@iPDA vaccine showed no tumor recurence (Figure 5L,M) whereas mice treated with PBS showed rapid tumor growth (Figure 5L,M). However, all mice show no tumor resistance to another type of tumor cells (4T1 cells) with rapidly growing tumors (Figure 5L,M; Figure S18, Supporting Information). These results indicate that *E. coli* (AH1-CDA-Co1)@iPDA vaccine could stimulate long-term antigen-specific immune memory.

In addition, the isolated splenocytes were analyzed by flow cytometry for the proportion of central memory T cells (Tcm) and effector memory T cells (Tem) on day 30. As shown in Figure 5N–P, the spleen of mice after oral administration of *E. coli* (AH1-CDA-Co1)@iPDA vaccine contained more Tcm ($CD3^+CD8^+CD44^+CD62L^+$), indicative of good long-term memory performance. In addition, there was no significant difference in Tem related to local immunity between these two groups, which may be due to the disappearance of local immunity induced by *E. coli* (AH1-CDA-Co1)@iPDA over a long period of time. Collectively, these results verify that *E. coli* (AH1-CDA-Co1)@iPDA tumor vaccine could induce effective immune memory for the prevention of tumor recurrence.

2.7. Antitumor Therapeutic Efficacy of *E. coli* (AH1-CDA-Co1)@iPDA in an Orthotopic Colon Tumor Model

To evaluate the translation potential of this oral vaccine of *E. coli* (AH1-CDA-Co1)@iPDA, a more clinically relevant orthotopic tumor model was established using luciferase labeled CT26 cells (CT26-Luc) (**Figure 6A**). Orthotopic tumor growth was confirmed by necropsy (Figure S19, Supporting Information) and bioluminescent 3D imaging (Figure 6B). This observation was confirmed from coronal, sagittal, transaxial, and full perspective angles. Ten days after orthotopic tumor implantation, mice were divided into six groups based on bioluminescence intensity and orally administered with different formulations every 7 days for three times (days 0, 7, and 14). Tumor growth was monitored by bioluminescent imaging every week (day 0, 7, 14, and 21) (Figure 6C).

Similar to PBS, *E. coli* (AH1-CDA-Co1) and *E. coli* (AH1-CDA-Co1)@iPDA (-US) barely inhibited tumor growth (Figure 6C,D). Of note, *E. coli* (AH1)@iPDA and *E. coli* (AH1-CDA)@iPDA showed a significant effect of inhibiting tumor growth (Figure 6C,D; Figures S20 and S21, Supporting Information), but tumors in the *E. coli* (AH1-CDA-Co1)@iPDA group regressed most (Figure 6C,D). At the end of the experiment (day 21), mice were euthanized, and tumors were excised. The weight of tumor from mice immunized with *E. coli* (AH1-CDA-Co1)@iPDA was 13.5–84.7-fold less than other control groups (Figure 6E). Also, the body weight of mice in all groups did not change significantly during the treatment period (Figure 6F). In addition, flow cytometry was used to analyze the immune cell infiltration in the tumor tissues on day 21. The tumor tissues after *E. coli* (AH1-CDA-Co1)@iPDA immunization contained the highest proportion of mature DCs and $CD8^+$T cells (Figure 6G,H). The content of $CD8^+$T cells in the tumor tissues of mice treated with *E. coli* (AH1-CDA-Co1)@iPDA was 1.6–31.8 fold higher than other control groups (Figure 6H). In particular, the tumor tissues of mice in the PBS group showed only ≈0.56% $CD8^+$T cell infiltration. In contrast, the T cell infiltration rate in the *E. coli* (AH1-CDA-Co1)@iPDA treatment group was 17.9%. And the total number of T cells increased by about30 times (Figure 6H). In addition, the number of immunosuppressive cells such as Treg cells and M2 macrophages in the tumor tissue was significantly reduced, indicating that *E. coli* (AH1-CDA-Co1)@iPDA immunization alleviated the immunosuppressive microenvironment and enhanced the antitumor effect of immune cells. These results collectively showed that the OMV (AH1-CDA-Co1) secreted from *E. coli* (AH1-CDA-Co1)@iPDA with the induction of US exhibited potent antitumor effect on orthotopic colorectal tumor.

2.8. Inhibition of Postoperative Tumor Recurrence by *E. coli* (AH1-CDA-Co1)@iPDA in an SLN-Metastasized Orthotopic Tumor Model

Metastasis to the sentinel lymph nodes (SLNs) is a common clinical issue after tumor resection, leading to tumor recurrence seriously affecting the prognosis of treatment.[29] Lymph node resection is still the mainstay approach to lymph node metastasis,[30] but incomplete lymph node resection may eventually lead to further tumor recurrence, whereas excessive resection might cause postoperative complications, such as infection, phlebitis, nerve damage and lymphedema.[31] Therefore, the ideal option is to control postoperative tumor recurrence without resection of SLNs. To investigate whether oral *E. coli* (AH1-CDA-Co1)@iPDA tumor vaccine could also control tumor recurrence without SLN removal, a model of orthotopic colon cancer with metastatic SLNs (specifically mesenteric lymph nodes, MLNs) was established. When tumor cells were inoculated for 20 days (on -20 day), tumor cells were found in MLNs to confirm the successful establishment of the SLNs metastasis model (Figure S22, Supporting Information). Therefore, the mice were subjected to surgical tumor

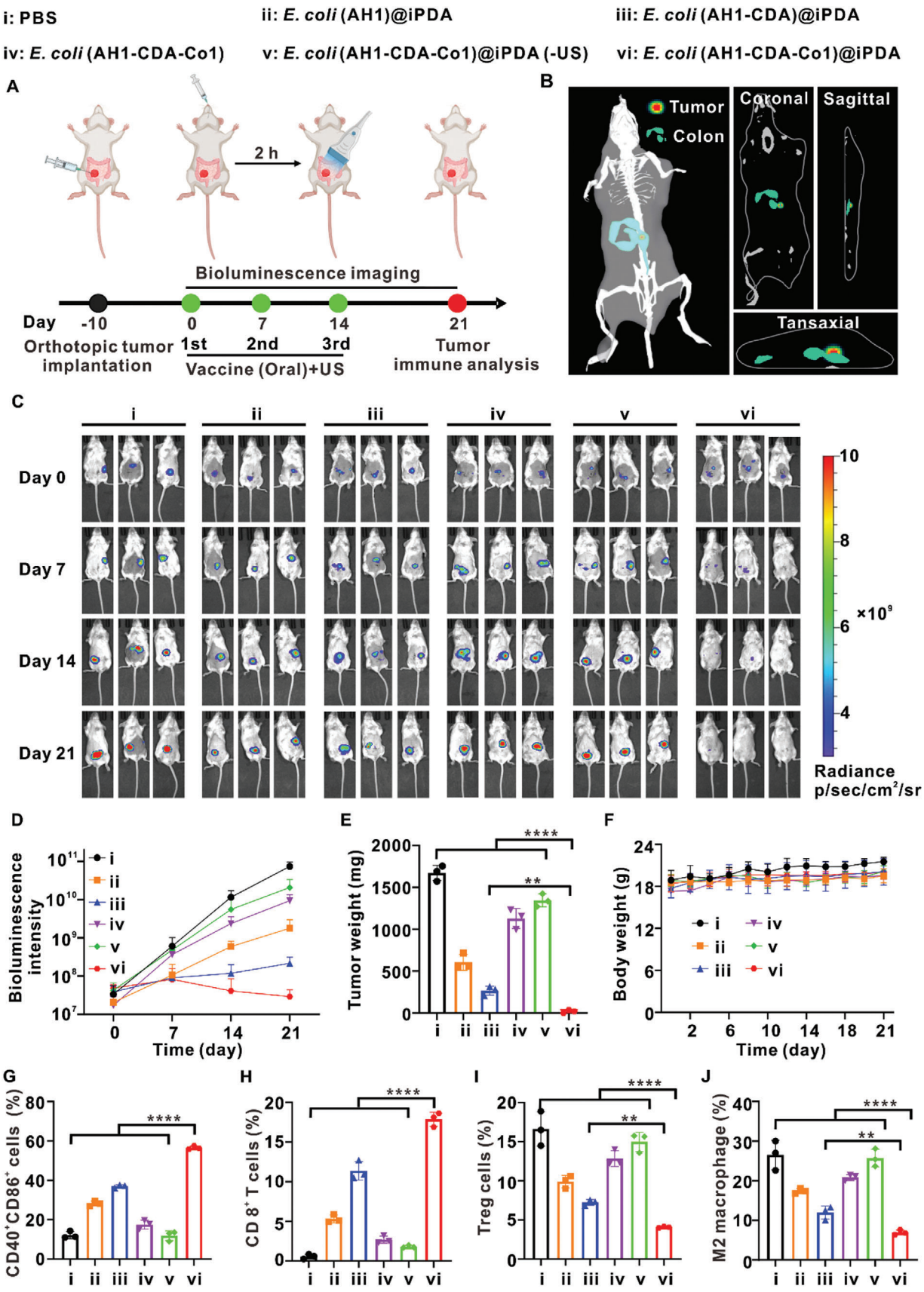

resection on day 0. Different formulations were orally administered on day 1, 8, and 15 for three times (**Figure 7A**). For comparison, a mixture of adjuvant polyinosinic-polycytidylic acid (Poly(I:C)) and antigen peptide AH1 (Poly(I:C)+AH1), as a common formulation in clinical trials, was subcutaneously injected as a positive control.[32]

In the PBS group, mice were euthanized when the total bioluminescence intensity of all tumors reached 3×10^{10} p s^{-1} (after day 29), and all mice were euthanized on day 32 (Figure 7B–E). Although the positive control extended the survival time of mice from day 30 to day 60, the survival rate of mice immunized with *E. coli* (AH1-CDA-Co1)@iPDA was as high as 100% on day 64 (Figure 7E). More importantly, 33% mice did not show recurrence after treatment by *E. coli* (AH1-CDA-Co1)@iPDA (Figure 7E), demonstrating that the oral vaccine has higher rate in controlling postoperative recurrence of orthotopic colon cancer than clinical formulation. Notably, the body weight of all groups did not change significantly during treatment (Figure 7F). In addition, the function of immune cells in metastatic MLNs is inhibited by invading tumor cells, such as the expression of vascular endothelial growth factor C, which promotes tumor-specific $CD8^+$ T cell dysfunction, and Treg cell expansion.[33] Therefore, MLNs were digested into single-cell suspensions for further cytometric analysis of immune cell infiltration and tumor cell counts on day 29. As expected, the number of tumor cells, Treg cells, and M2 macrophages in the MLNs in the *E. coli* (AH1-CDA-Co1)@iPDA group were significantly lower than that of the Poly(I:C)+AH1 vaccination group and PBS group (Figure 7G–L). The proportion of mature DCs, $CD8^+$T and $CD4^+$ T cells in the MLN in the *E. coli* (AH1-CDA-Co1)@iPDA group significantly increased than that Poly(I:C)+AH1 and PBS group (Figure 7G–L). These results further confirmed that *E. coli* (AH1-CDA-Co1)@iPDA could effectively activate antigen-specific immune responses and reprogram microenvironment in MLNs to potentially avoid resection of metastasized LNs.

3. Conclusion

In summary, we designed an US-mediated, genetically engineered commensal bacteria system that can precisely regulate secretion of OMVs containing tumor antigens, adjuvants and targeting peptides as an in situ oral vaccine for colon cancer treatment. As such, sustained secretion of OMVs in the intestine was achieved by iPDA coating on bacteria. *E. coli* (AH1-CDA-Co1)@iPDA enables to enter PPs via M cell to trigger long-term and tumor-specific immune memory responses. Importantly, significant inhibition tumor growth with prolonged survival rate and no tumor reoccurrence were observed in subcutaneous, orthotopic and metastasis tumor models. Taken together, *E. coli* (AH1-CDA-Co1)@iPDA holds potential as a potent oral tumor vaccine for cancer immunotherapy.

4. Experimental Section

Animals and Cells: Female BALB/c (6–8 weeks old) were obtained from Beijing Vital River Laboratory Animal Technology Co., Ltd. All the animal procedures were approved by the Animal Experiment Ethics Committee at the Tianjin University. Mice were housed in a room at 20–22 °C with a 12 h light/dark cycle and at 30–70% humidity.

Caco-2 cells were purchased from Wuhan SUNNCELL Biotechnology Co., Ltd. DC2.4 cells and RAW264.7 cells were purchased from AoRuisai Biotechnology Co., Ltd. CT26 (BNCC287983) were purchased from the Beijing BeNa Culture Collection. The cells were cultured in 1640 or DMEM medium with 100 U mL^{-1} of streptomycin and penicillin (BioChannel Biological Technology Co., Ltd.), and 10% fetal bovine serum (Yeasen, Shanghai, China) at 37 °C in a humidified incubator with 5% CO_2.

Evaluation of Ultrasonic Performance: To study the heat generation performance of US, US was irradiated at different powers (1, 2, 3, 4, 5, and 7 W) into the 6-well plate containing culture medium and the mouse abdominal cavity for different periods of time. All temperature changes during the irradiation process were detected by an infrared thermal imager.

Plasmid Construction and Preparation of US-Responsive Bacterium: The all plasmids (pBV220-AH1, pBV220-AH1-CDA, pBV220-AH1-CDA-Co1, and pBV220-mCherry) were constructed and provided from MiaoLingBio, China. In brief, the AH1-CDA-Co1 gene connected by enzyme digestion of the OmpA secretion signal sequence was inserted into the pBV220 plasmid to generate a thermosensitive plasmid expressing AH1-CDA-Co1 (pBV220-AH1-CDA-Co1). The recombinant plasmid was transformed into *E. coli* 1917 competent cells by chemical transformation. At the same time, a thermosensitive control plasmid expressing AH1 (pBV220-AH1), AH1-CDA (pBV220-AH1-CDA), mCherry (pBV220-mCherry) was constructed to facilitate the detection of gene expression. The pBV220-AH1-CDA-Co1 or pBV220-mCherry plasmid was chemically transformed into Escherichia coli 1917 strains to obtain US-responsive bacteria.

Thermal-Induced and US-Induced mCherry and MYC Expression: US-sensitive bacteria were incubated at 37 or 45 °C for 30 min and further incubated at 37 °C for different times. The fluorescence signal of bacteria and MYC protein expression were detected by IVIS spectroscopy and western blot, respectively. To verify the feasibility of US-induced mCherry gene expression in vivo, US-sensitive bacteria were orally administered for 2 h, and the mouse peritoneum was irradiated with US for 20 min. After 2 h, the fluorescence intensity of the mouse peritoneum was detected by IVIS. Subsequently, the mice were euthanized and the intestines were removed for separate IVIS imaging.

OMVs Preparation and Characterization: After culturing the different engineered bacteria at 30 °C for 12 h, the OD_{600} was diluted to 0.1. The cells were stimulated at 37 or 45 °C for 30 min and then cultured at 37 °C for 12 h. The supernatant was collected by centrifugation for 30 min (4 °C, 5000 × g), which was filtered through a 0.45 µm polyvinylidene fluoride filter and concentrated by a 50 kDa ultrafiltration membrane. The concentrated solution was filtered again by a 0.22 µm filter and collected by ultracentrifugation at 150 000× g for 3 h at 4 °C. The pellet was finally resuspended in PBS and passed through a 0.22 µm filter to remove intact bacteria or cell debris. The filtrate was stored at −80 °C for further use. The

Figure 6. Antitumor efficacy of *E. coli* (AH1-CDA-C1)@iPDA in an orthotopic colorectal tumor model. A) Schematic illustration of orthotopic colorectal cancer implantation and oral immunotherapy. The oral vaccination dose is 1×10^8 CFU. B) The images of orthotopic CT26-Luc tumors observed from the coronal, sagittal, and transaxial perspectives by 3D IVIS. C) In vivo bioluminescence imaging of CT26-Luc tumor at the indicated time. D) Tumor growth profiles by quantifying the bioluminescence in panel C ($n = 3$). E) Tumor weight on the last day (day 21) of the test ($n = 3$). F) Body weight of mice ($n = 3$). G–J) The infiltrating immune cells in the orthotopic colorectal tumor tissues were detected by flow cytometry, including mature DC($CD11c^+CD40^+CD86^+$), $CD3^+CD8^+$ T cells, Treg cells ($CD3^+CD4^+Foxp3^+$), M2 macrophages ($F4/80^+CD206^+$). i: PBS, ii: *E. coli* (AH1)@iPDA, iii: *E. coli* (AH1-CDA)@iPDA, iv: *E. coli* (AH1-CDA-Co1), v: *E. coli* (AH1-CDA-Co1)@iPDA (-US) and vi: *E. coli* (AH1-CDA-Co1)@iPDA. Data are represented as mean ± S.D. $n = 3$; Statistical significance was calculated via one-way ANOVA with Turkey's test: $^{ns}p > 0.05$; $^{*}p < 0.05$; $^{**}p < 0.01$; $^{***}p < 0.001$; $^{****}p < 0.0001$.

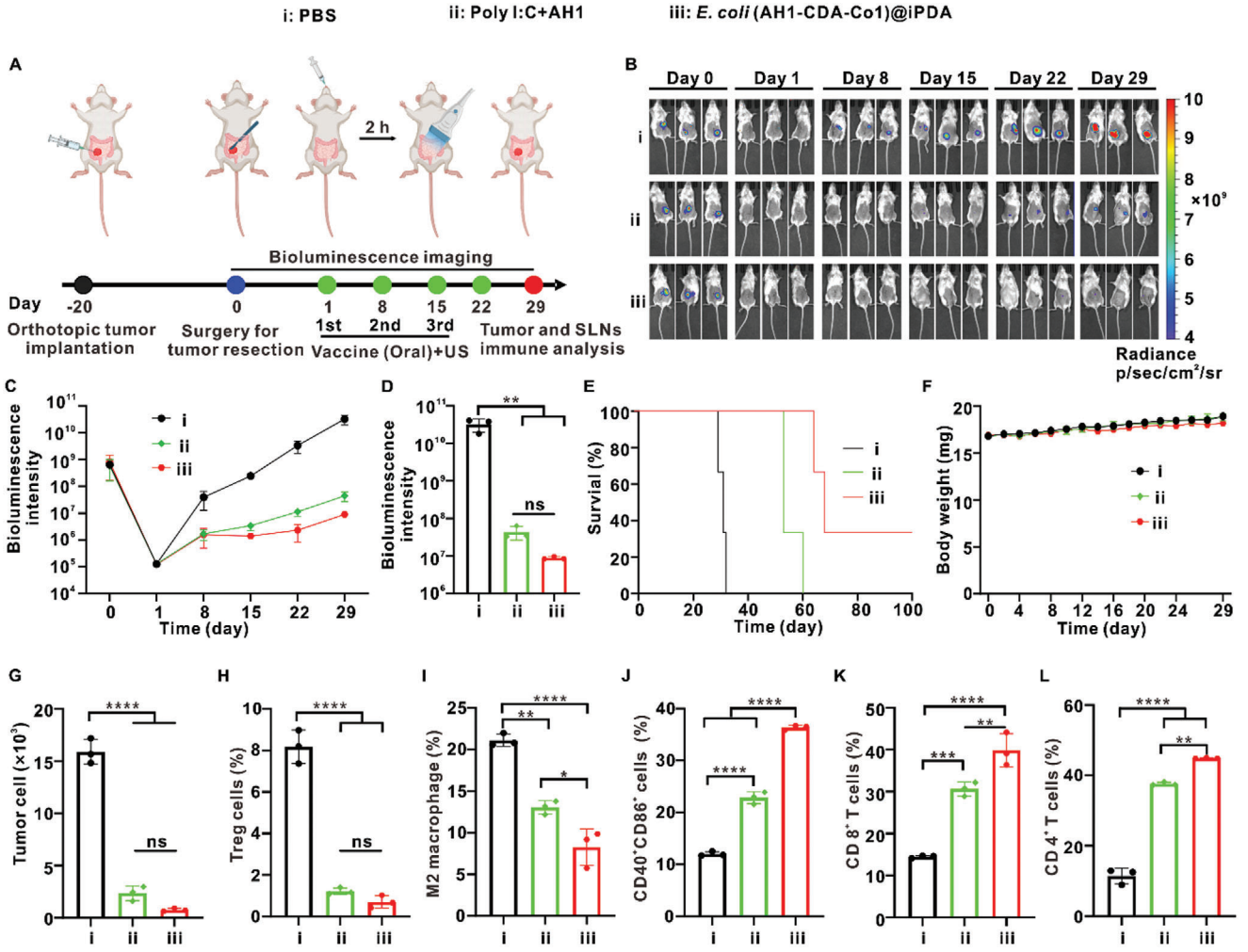

Figure 7. Management of postoperative tumor resection effect by *E. coli* (AH1-CDA-Co1)@iPDA in a sentinel lymph node metastasized orthotopic tumor model. A) Schematic illustration of oral immunotherapy. The oral immunization dose is 1×10^8 CFU. B) In vivo bioluminescence imaging of CT26-Luc tumor at the indicated time. C,D) Tumor growth profiles by quantifying the bioluminescence in panel C ($n = 3$). E) Survival rate of the mice. And F) Body weight of mice after treatments as indicated ($n = 3$). G) Tumor cell counts in MLNs quantified by flow cytometry. H–L) The infiltrating immune cells in the MLNs were detected by flow cytometry, including Treg cells ($CD3^+CD4^+Foxp3^+$), M2 macrophages ($F4/80^+CD206^+$), mature DC($CD11c^+CD40^+CD86^+$), $CD3^+CD8^+$ T cells and $CD3^+CD4^+$ T cells. i: PBS, ii Poly(I:C) + AH1: iii: *E. coli* (AH1-CDA-Co1)@iPDA. Data are represented as mean ± S.D. $n = 3$; Statistical significance was calculated via one-way ANOVA with Turkey's test: $^{ns}p > 0.05$; $^{*}p < 0.05$; $^{**}p < 0.01$; $^{***}p < 0.001$; $^{****}p < 0.0001$.

morphology of OMVs was characterized by transmission electron microscopy, and OMVs were analyzed by Western blot.

Western Blot Analysis: Western blotting was used to verify protein expression in OMVs and activation of the STING pathway in immune cells. OMVs and cells were lysed by adding radioimmunoprecipitation assay (RIPA) buffer (Beyotime) and total protein concentration was quantified using the Pierce BCA protein assay kit (Thermo Fisher scientific). Equal amounts of protein (30 μg) were separated by SDS-polyacrylamide gel and electro-transferred from the gel to a polyvinylidene fluoride (PVDF) membrane. The membrane was then blocked with 5% skim milk and incubated with specific primary antibodies at 4 °C overnight or at room temperature for 2 h, including [MYC (Abways techology), phospho-NF-κB p65 (pS536) (Abways techology), NF-κB p65 (Abways techology), phospho-IRF3 (pS396) (Abways techology), IRF3 (Abways techology), phospho-TBK1 (pS172) (Abways techology), TBK1 (Abways techology), or GAPDH (Abways techology)]. Then the corresponding secondary antibodies were added and incubated at room temperature for 2 h. Chemiluminescence detection was performed using Enhanced ECL Chemiluminescence Kit (Biodragon) to visualize the protein bands, and the protein bands were quantified using ImageJ software.

OMVs Translocation by M Cells In Vitro: OMVs crossing intestinal epithelial cells was measured in vitro by using a transwell system. Caco-2 cells (5×10^5) were seeded in the upper chamber of the transwell and cultured for 14 days, with the medium replaced every 2 days. OMVs were labeled with 3,3′-dioctadecyl oxalocyanine(DiO) (US EVERBRIGHT, Suzhou, China). DiO-labeled OMV (AH1), OMV (AH1-CDA), OMV (AH1-CDA-Co1) (-US) or OMV (AH1-CDA-Co1) were added to the upper chamber. Fluorescence intensity in the lower chamber was measured 12 h later.

Evaluation of the Immune Effect of OMVs In Vitro: Bone marrow-derived dendritic cells (BMDCs) were extracted according to the method reported previously. Briefly, BMDCs were extracted from the femurs of 6–8 weekly old female BALB/c mice, and the collected bone marrow was added to the erythrocyte lysis buffer to lyse the erythrocytes. BMDCs were then cultured in 1640 medium containing GM-CSF (20 ng mL^{-1}) (Genscript).

The medium was replenished after the fourth day of culture. Caco-2 cells (5×10^5) were seeded in the upper chamber of the transwell and cultured for 14 days, and then BMDCs were seeded in the lower chamber of the transwell. After 10 h, OMVs from different engineered bacteria were added to the upper chamber and cultured for 48 h.

BMDCs incubated with lipopolysaccharide were used as the positive control. After staining with APC anti-mouse CD11c, FITC anti-mouse CD40 and Percp-Cy5.5 anti-mouse CD86 antibodies, BMDCs were analyzed by flow cytometry (CytoFLEX) to detect BMDCs maturation.

The mature BMDCs obtained above were then cocultured with APC-stained $CD8^+$ T cells, isolated from the spleen of C57BL/6J mice using APC anti-mouse CD8 antibody screening. After 72 h of coculture, cells were collected and stained with FITC anti-mouse CD3 and PE anti-mouse CD62L antibodies for flow cytometry. Culture medium was filtered and collected for measurement of TNF α, IFN β and IL-12p70 using ELISA kit (Solarbio and Amoy Lunchangshuo Biotech, Co., Ltd).

DCs or T cells treated with different OMVs were subjected to migration assay by using a 24-Transwell plate. Immune cells were seeded in the upper chamber, and the lower chamber was filled with CT26 cells. After incubation for 3 h, immune cells migrated into the bottom chamber were counted using flow cytometry (CytoFLEX).

These proliferated effector $CD8^+$ T cells were cocultured with tumor cells (CT26 or 4T1) in 96-well plates for 72 h. The apoptosis/necrosis of tumor cells were analyzed by enhanced CCK-8 assay kit (CT0001; Shandong Sparkjade Biotechnology Co., Ltd.).

Evaluation of OMVs Intestinal Epithelium Penetration and Targeting to PPs: Mice were fasted for 6 h and anesthetized, and the intestinal loop containing PPs (≈2 cm long) was ligated with thread. Fifty micrograms of DiO-labeled OMV (AH1), OMV (AH1-CDA), OMV (AH1-CDA-Co1) (-US), or OMV (AH1-CDA-Co1) was injected into the ligated intestinal lumen. 2 h later, mice were euthanized, and PPs and intestinal epithelial cells were collected for fluorescence detection. In addition, the PPs were collected for immunofluorescent staining analyses. Frozen sections (10–15 mm in thickness) of PPs from BALB/c mice, obtained using a cryomicrotome, were fixed with 4% paraformaldehyde, blocked with 2.5% BSA/PBS, and stained with rhodamine-UEA-1 (Ulex Europaeus Agglutinin I) (Shanghai Maokang Biotechnology Co., Ltd.). Finally, the sections were counterstained with DAPI and analyzed by CLSM.

Bacteria@iPDA Solution Preparation: Bacteria or fluorescently labeled bacteria were encapsulated in PDA, and chemical cross-linking was achieved using reactive groups on the surface of PDA to incorporate bacteria into the PDA coating layer. Specifically, bacteria (1×10^8) were added to tris buffer (100 mM, 2 mL, pH 8.5), and dopamine (4 mg) was quickly added. The reaction mixture was kept and stirred (800 rpm) at room temperature for 2 h for oxidization of dopamine to form PDA. The synthesized PDA-bacterium was purified by centrifugation (3500 rpm × 5 min) to remove dopamine. For oral administration, as prepared PDA-bacterium was resuspended in 0.2 mL tris buffer (100 mM, pH 8.5), and dopamine hydrochloride (2 mg) and small amount of hydrogen peroxide (30%, 2 µL) were quickly added to further form PDA coating occurring in situ on the surface of intestines for prolonged bacterial transit time in intestine. The mixed three-buffered iPDA solution was used fresh for following animal experiments.

Evaluation of the Intestinal Residence Time of Bacterial iPDA Solution In Vivo: To detect the iPDA system to enhance the intestinal residence time, probiotics were fluorescently labeled. The introduction of azide moieties onto the bacterial surface via metabolic oligosaccharide engineering, transformed bacteria were grown to mid-log phase in LB medium containing kanamycin, ampicillin, and 50 µM Ac4GalNAz at 37 °C with shaking (180 rpm). After 12 h, the probiotics were collected by centrifugation and washed twice with PBS, and DBCO-Cy5 was added for staining for 30 min.

After the mice were fasted for 10 h, the fluorescently labeled probiotics were administered to the mice via the iPDA system. Fluorescence imaging (IVIS Spectrum) was used to monitor the fluorescence intensity of the mouse peritoneal cavity at 2, 4, 7, 10, and 24 h. The mice were euthanized after 24 h, and the intestines were removed for IVIS fluorescence imaging alone.

In Vivo Immune Stimulation by Oral Vaccines and Isolation of PPs Lymphocytes: To evaluate the antitumor effect of oral vaccines in solid tumor models, 2×10^6 CT26 cells were injected subcutaneously into the left flank of BALB/c mice on day -10. Mice were orally inoculated with PBS, *E. coli* (AH1)@iPDA, *E. coli* (AH1-CDA)@iPDA, *E. coli* (AH1-CDA-Co1), *E. coli* (AH1-CDA-Co1)@iPDA(-US), or *E. coli* (AH1-CDA-Co1)@iPDA on days 0, 7, and 14 ($n = 5$). The CFU of oral bacteria is 1×10^8. If applicable, mice were irradiated with US for 20 min 2 h after each administration. The mice were euthanized on day 21, and lymphocytes from tumors, inguinal lymph nodes, and spleens were collected using spleen lymphocyte separation medium (Dakewe Biotech Co., Ltd, Shenzhen, China) and tumor infiltrating tissue lymphocyte separation fluid kit (Solarbio, Beijing, China) and flow cytometry analysis of immune cells (DC, T cell, NK cell, macrophage) was performed. serum was used to detect the expression of IFN β ELISA kits (Amoy Lunchangshuo Biotech, Co., Ltd) and TNF α ELISA kits (Solarbio, Beijing, China). The AH1 peptide was synthesized by Genscript.

In Vivo Antitumor Therapy Using OMVs Vaccine in Suit in Mice Bearing Subcutaneous CT26 Colorectal Tumor: To evaluate the antitumor effect of oral vaccines in solid tumor models, 2×10^6 CT26 cells were injected subcutaneously into the left flank of BALB/c mice on day -10. Mice were orally administered with PBS, *E. coli* (AH1)@iPDA, *E. coli* (AH1-CDA)@iPDA, *E. coli* (AH1-CDA-Co1), *E. coli* (AH1-CDA-Co1)@iPDA(-US), or *E. coli* (AH1-CDA-Co1)@iPDA on days 0, 7, and 14 ($n = 5$). The CFU of oral bacteria is 1×10^8. If applicable, mice were irradiated with US for 20 min 2 h after each administration. The body weight and tumor volume of mice were measured daily and calculated according to the following formula: tumor volume = (tumor length) × (tumor width)2×0.5. Mice were euthanized when the tumor volume reached 1200 mm^3.

Subcutaneous CT26 Colorectal Tumor Rechallenge: In the re-challenge experiment, mice that survived long term after *E. coli* (AH1-CDA-Co1)@iPDA treatment ($n = 3$) were subcutaneously injected with 2×10^6 CT26 cells (left) and 2×10^6 4T1 cells (right) on day 70. Additional control mice ($n = 3$) were implanted with the same tumor to confirm tumor growth. Tumor volume was measured and calculated longitudinally with a vernier caliper for up to 30 days. The tumor volume was calculated according to the formula tumor volume = (tumor length) × (tumor width)^2 × 0.5.

CD8 T Cell Depletion: The tumor model was established according to previously reported methods.[34] Briefly, 2×10^6 CT26 cells were injected subcutaneously into the left flank of BALB/c mice on day -7. On day 0, 2, 6, 8, 14, and 16, mice were intraperitoneally injected with the purified anti-mouse CD8a antibody (Biolegend, USA) at a dose of 100 µg. Mice were individually treated with PBS, *E. coli* (AH1-CDA-Co1)@iPDA plus anti-CD8 antibody, *E. coli* (AH1-CDA-Co1)@iPDA on day 4, 11, and 18 ($n = 4$). Tumor volume was measured every other day. Mice were sacrificed when the tumor size reached 1500 mm^3 or when animals became moribund with severe weight loss or ulceration. The tumor volume was calculated according to the formula tumor volume = (tumor length) × (tumor width)$^2 \times 0.5$.

In Vivo Antitumor Therapy Using OMVs Vaccine in Suit in Mice Bearing Orthotopic Colorectal Tumor: The orthotopic colon cancer model was established in female BALB/c mice as described previously. Female BALB/c mice (6–8 weeks old) were anesthetized by intraperitoneal injection of 5% chloral hydrate solution. The abdomen was disinfected with an alcohol swab. Then a midline incision was made through the lower flank, and the cecum was removed. A suspension of 1×10^7 CT26-Luc cells in 50 µL serum-free 1640 medium containing 10 µg μL^{-1} matrix was injected into the cecal wall. To prevent leakage, a cotton swab was carefully held at the injection site for 1 min. The cecum was returned to the peritoneal cavity, and the peritoneum and skin were sutured separately. Ten days after orthotopic tumor cell inoculation (intraperitoneal bioluminescence intensity was $\approx 1 \times 10^8$ p s^{-1}), the tumor-bearing mice were randomly divided into six groups ($n = 3$) according to the tumor bioluminescence intensity. Mice were orally inoculated with PBS, *E. coli* (AH1)@iPDA, *E. coli* (AH1-CDA)@iPDA, *E. coli* (AH1-CDA-Co1), *E. coli* (AH1-CDA-Co1)@iPDA(-US), or *E. coli* (AH1-CDA-Co1)@iPDA on days 0, 7, and 14 ($n = 3$). The CFU of oral bacteria is 1×10^8. If applicable, mice were irradiated with US for 20 min 2 h after each administration. Tumor burden was monitored weekly

using bioluminescent imaging by injecting D-Luciferin, Sodium Salt (US EVERBRIGHT, Suzhou, China). Body weights were recorded throughout the study. Mice were euthanized at the end of the study (day 21), and tumors were removed and weighed.

Identifying Tumor Metastasis in Sentinel Lymph Node: To identify sentinel lymph node metastasis, the same orthotopic colon cancer model by inoculating CT26-Luc cells was established. On day 20 after inoculation, sentinel lymph nodes (mesenteric lymph nodes) were collected and immediately subjected to bioluminescence imaging.

In Vivo Postsurgical Therapy Using OMVs Vaccine in Suit in Orthotopic Colorectal Tumor Model with Orthotopic Sentinel Lymph Node Metastasis: To investigate the therapeutic effect of oral tumor vaccine on inhibiting the recurrence of postoperative orthotopic colon cancer, the orthotopic colon cancer tumor model was established by inoculating 2×10^6 CT26-Luc cells in situ using the above method. On the 20th day after inoculation, the orthotopic colon tumors of mice were resected and randomly divided into three groups. Mice were orally administered with PBS and *E. coli* (AH1-CDA-Co1)@iPDA on day 1, 8, and 15 ($n = 3$). Mice treated with PBS served as the negative control group. Mice immunized subcutaneously with a mixture of 50 µg adjuvant Poly (I:C)+ 50 µg AH1 peptide (Genscript) served as the positive control group. The CFU of oral bacteria is 1×10^8.

Statistical Analysis: Data were represented as mean ± standard deviation (S.D.). Flow cytometry results were analyzed by FlowJo v10. The statistical significance via the one-way ANOVA with Tukey's test and log-rank test, respectively or two-tailed multiple *t*-tests with Bonferroni–Dunn correction. The level of significance was defined at $^{ns}p > 0.05$; $^{*}p < 0.05$, $^{**}p < 0.01$, $^{***}p < 0.001$, $^{****}p < 0.0001$. All statistical analyses were performed using GraphPad Prism 8.0 software. All the data supporting the findings of this study are available within the article and its supplementary information files and from the corresponding author upon reasonable request. A reporting summary for this article is available as a Supplementary Information file.

Supporting Information

Supporting Information is available from the Wiley Online Library or from the author.

Acknowledgements

This work was supported by the National Natural Science Foundation of China (22375144; 32071384) and the National Key Research and Development Program (2021YFC2102300).

Conflict of Interest

The authors declare no conflict of interest.

Author contributions

J.L. and R.Y. contributed equally to this work. J.L.and Y.Z. conceived the project. J.L. and R.Y. carried out the most experiments. H.R. assisted with material synthesis and animal experiments. J.H. assisted with bacterial construction. Y.Y. and C.F. assisted with orthotopic model establishment. J.L., R.Y. and Y.Z. performed data analysis and wrote the manuscript. J.F.L. assisted with manuscript editing.

Data Availability Statement

The data that support the findings of this study are available in the supplementary material of this article.

Keywords

cGAS-STING pathway, M-cell targeting, oral immunotherapy, outer membrane vesicles, residence time, ultrasound

Received: August 16, 2024
Revised: November 25, 2024
Published online:

[1] a) C. Xiao, X. Zhao, X. Li, S. Zhu, J. Cao, H. Chen, D. Li, L. Sha, F. Huang, Z. Hei, *Clin. Transl. Oncol.* **2023**, *25*, 491; b) C. Eng, A. A. Jácome, R. Agarwal, M. H. Hayat, M. X. Byndloss, A. N. Holowatyj, C. Bailey, C. H. Lieu, *Lancet Oncol.* **2022**, *23*, e116; c) K. Bibbins-Domingo, D. C. Grossman, S. J. Curry, K. W. Davidson, J. W. Epling, F. A. R. García, M. W. Gillman, D. M. Harper, A. R. Kemper, A. H. Krist, A. E. Kurth, C. S. Landefeld, C. M. Mangione, D. K. Owens, W. R. Phillips, M. G. Phipps, M. P. Pignone, A. L. Siu, U. S. P. S. T. Force, *Jama-J. Am. Med. Assoc.* **2016**, *315*, 2564.

[2] a) Y. Yue, J. Xu, Y. Li, K. Cheng, Q. Feng, X. Ma, N. Ma, T. Zhang, X. Wang, X. Zhao, *Nat. Biomed. Eng.* **2022**, *6*, 898; b) X. Cao, Y. Xu, C. Zhou, J. Huo, S. Su, L. Liu, Z. Zhu, L. Li, W. Jia, C. Wang, *Adv. Sci.* **2023**, *10*, 2302910; c) V. Gopalakrishnan, C. N. Spencer, L. Nezi, A. Reuben, M. C. Andrews, T. V. Karpinets, P. A. Prieto, D. Vicente, K. Hoffman, S. C. Wei, A. P. Cogdill, L. Zhao, C. W. Hudgens, D. S. Hutchinson, T. Manzo, M. P. de Macedo, T. Cotechini, T. Kumar, W. S. Chen, S. M. Reddy, R. S. Sloane, J. Galloway-Pena, H. Jiang, P. L. Chen, E. J. Shpall, K. Rezvani, A. M. Alousi, R. F. Chemaly, S. Shelburne, L. M. Vence, et al., *Science* **2018**, *359*, 97; d) K. Han, J. Nam, J. Xu, X. Sun, X. Huang, O. Animasahun, A. Achreja, J. H. Jeon, B. Pursley, N. Kamada, *Nat. Biomed. Eng.* **2021**, *5*, 1377; e) Y. Zhang, M. Li, G. Du, X. Chen, X. Sun, *Adv. Drug Delivery Rev.* **2021**, *177*, 113928; f) K. Han, F. Xie, O. Animasahun, M. Nenwani, S. Kitamoto, Y. Kim, M. T. Phoo, J. Xu, F. Wuchu, K. Omoloja, *Nat. Mater.* **2024**, 1.

[3] R. New, *Clin. Exp. Immunol.* **2019**, *198*, 153.

[4] a) S. H. Kim, Y. S. Jang, *Exper. Mol. Med.* **2014**, *46*, e85; b) T. Nochi, Y. Yuki, A. Matsumura, M. Mejima, K. Terahara, D. Y. Kim, S. Fukuyama, K. Iwatsuki-Horimoto, Y. Kawaoka, T. Kohda, S. Kozaki, O. Igarashi, H. Kiyono, *J. Exp. Med.* **2007**, *204*, 2789.

[5] A. Mullard, *Nat. Rev. Drug Discovery* **2020**, *19*, NA.

[6] a) C. L. Ho, H. Q. Tan, K. J. Chua, A. Kang, K. H. Lim, K. L. Ling, W. S. Yew, Y. S. Lee, J. P. Thiery, M. W. Chang, *Nat. Biomed. Eng.* **2018**, *2*, 27; b) D. W. Zheng, R. Q. Li, J. X. An, T. Q. Xie, Z. Y. Han, R. Xu, Y. Fang, X. Z. Zhang, *Adv. Mater.* **2020**, *32*, 2004529.

[7] a) M. Li, H. Zhou, W. Jiang, C. Yang, H. Miao, Y. Wang, *Nano Today* **2020**, *35*, 101007; b) M. Kaparakis-Liaskos, R. L. Ferrero, *Nat. Rev. Immunol.* **2015**, *15*, 375; c) R. Stentz, A. L. Carvalho, E. J. Jones, S. R. Carding, *Biochem. Soc. Trans.* **2018**, *46*, 1021.

[8] a) Y. Li, R. Zhao, K. Cheng, K. Zhang, Y. Wang, Y. Zhang, Y. Li, G. Liu, J. Xu, J. Xu, *ACS Nano* **2020**, *14*, 16698; b) K. Cheng, R. Zhao, Y. Li, Y. Qi, Y. Wang, Y. Zhang, H. Qin, Y. Qin, L. Chen, C. Li, *Nat. Commun.* **2021**, *12*, 2041.

[9] a) X. Ma, X. Liang, Y. Li, Q. Feng, K. Cheng, N. Ma, F. Zhu, X. Guo, Y. Yue, G. Liu, *Nat. Commun.* **2023**, *14*, 1606; b) N. D. Taylor, A. S. Garruss, R. Moretti, S. Chan, M. A. Arbing, D. Cascio, J. K. Rogers, F. J. Isaacs, S. Kosuri, D. Baker, *Nat. Methods* **2016**, *13*, 177.

[10] a) S. Sun, Q. Tang, L. Sun, J. Zhang, L. Zhang, M. Xu, J. Chen, M. Gong, X. Liang, *Mater. Today Adv.* **2022**, *14*, 100248; b) A. Carpentier, M. Canney, A. Vignot, V. Reina, K. Beccaria, C. Horodyckid, C. Karachi, D. Leclercq, C. Lafon, J. Y. Chapelon, L. Capelle, P. Cornu, M. Sanson, K. Hoang-Xuan, J. Y. Delattre, A. Idbaih, *Sci. Transl. Med.* **2016**, *8*, 343re2; c) S. Son, J. H. Kim, X. W. Wang, C. L. Zhang, S. A. Yoon, J. Shin, A. Sharma, M. H. Lee, L. Cheng, J. S. Wu, J. S. Kim, *Chem.*

Soc. Rev. **2020**, *49*, 3244; d) J. Deprez, G. Lajoinie, Y. Engelen, S. C. De Smedt, I. Lentacker, *Adv. Drug Delivery Rev.* **2021**, *172*, 9.
[11] H. J. Hu, X. Zhu, C. H. Wang, L. Zhang, X. S. Li, S. Lee, Z. L. Huang, R. M. Chen, Z. Y. Chen, C. F. Wang, Y. Gu, Y. M. Chen, Y. S. Lei, T. J. Zhang, N. Kim, Y. X. Guo, Y. Teng, W. B. Zhou, Y. Li, A. Nomoto, S. Sternini, Q. F. Zhou, M. Pharr, F. L. di Scalea, S. Xu, *Sci. Adv.* **2018**, *4*, eaat0292.
[12] C. Zhang, K. Pu, *Adv. Mater.* **2023**, *35*, 2303059.
[13] M. H. Abedi, M. S. Yao, D. R. Mittelstein, A. Bar-Zion, M. B. Swift, A. Lee-Gosselin, P. Barturen-Larrea, M. T. Buss, M. G. Shapiro, *Nat. Commun.* **2022**, *13*, 1585.
[14] S. Mitragotri, *Nat. Rev. Drug Discovery* **2005**, *4*, 255.
[15] a) M. G. Shapiro, P. W. Goodwill, A. Neogy, M. Yin, F. S. Foster, D. V. Schaffer, S. M. Conolly, *Nat. Nanotechnol.* **2014**, *9*, 311; b) R. W. Bourdeau, A. Lee-Gosselin, A. Lakshmanan, A. Farhadi, S. R. Kumar, S. P. Nety, M. G. Shapiro, *Nature* **2018**, *553*, 86.
[16] Y. Chen, M. Du, Z. Yuan, Z. Chen, F. Yan, *Nat. Commun.* **2022**, *13*, 4468.
[17] a) M.-R. Wu, B. Jusiak, T. K. Lu, *Nat. Rev. Cancer* **2019**, *19*, 187; b) J. L. Royo, P. D. Becker, E. M. Camacho, A. Cebolla, C. Link, E. Santero, C. A. Guzmán, *Nat. Methods* **2007**, *4*, 937; c) N. S. Forbes, *Nat. Rev. Cancer* **2010**, *10*, 785.
[18] a) W. Um, H. Ko, D. G. You, S. Lim, G. Kwak, M. K. Shim, S. Yang, J. Lee, Y. Song, K. Kim, *Adv. Mater.* **2020**, *32*, 1907953; b) X. Liang, J. Gao, L. Jiang, J. Luo, L. Jing, X. Li, Y. Jin, Z. Dai, *ACS Nano* **2015**, *9*, 1280; c) S. B. Devarakonda, M. R. Myers, M. Lanier, C. Dumoulin, R. K. Banerjee, *Nano Lett.* **2017**, *17*, 2532.
[19] a) Y. B. Miao, Y. J. Lin, K. H. Chen, P. K. Luo, S. H. Chuang, Y. T. Yu, H. M. Tai, C. T. Chen, K. J. Lin, H. W. Sung, *Adv. Mater.* **2021**, *33*, 2104139; b) S. Ferber, R. J. Gonzalez, A. M. Cryer, U. H. von Andrian, N. Artzi, *Adv. Mater.* **2020**, *32*, 1903847.
[20] a) S. H. Kim, K. W. Seo, J. Kim, K. Y. Lee, Y. S. Jang, *J. Immunol.* **2010**, *185*, 5787; b) F. D. Zhang, Z. W. Zhang, X. Li, J. H. Li, J. L. Lv, Z. Y. Ma, L. Pan, *Viruses-Basel* **2021**, *13*, eadj1736; c) T. Ngo-My, D. Nguyen-Le, T. T. Le, Q. G. Mai, H. V. Vo-Nguyen, A. H. N. Nguyen, K. L. T. Dao, K. T. Quang, H. T. T. Vu, T. T. T. Nguyen, H. Tran-Van, *Iranian J. Sci.* **2023**, *47*, 1049.
[21] a) M. J. Wright, G. C. Bai, *Mol. Microbiol.* **2023**, *120*, 791; b) D. S. Leventhal, A. Sokolovska, N. Li, C. Plescia, S. A. Kolodziej, C. W. Gallant, R. Christmas, J. R. Gao, M. J. James, A. Abin-Fuentes, M. Momin, C. Bergeron, A. Fisher, P. F. Miller, K. A. West, J. M. Lora, *Nat. Commun.* **2020**, *11*, 2739; c) J. Rismondo, J. Gibhardt, J. Rosenberg, V. Kaever, S. Halbedel, F. M. Commichau, *J. Bacteriol.* **2016**, *198*, 416; d) Y. L. Bai, J. Yang, X. Zhou, X. X. Ding, L. E. Eisele, G. C. Bai, *PLoS One* **2012**, *7*, e31251.
[22] C. Hilgendorf, H. Spahn-Langguth, C. G. Regårdh, E. Lipka, G. L. Amidon, P. Langguth, *J. Pharm. Sci.* **2000**, *89*, 63.
[23] Y. Yang, Y. Cheng, L. Cheng, *Trends Immunol.* **2024**, *45*, 549.
[24] a) P. Feng, Z. Cao, X. Wang, J. Li, J. Liu, *Adv. Mater.* **2020**, *32*, 2002406; b) Z. Cao, X. Wang, Y. Pang, S. Cheng, J. Liu, *Nat. Commun.* **2019**, *10*, 5783; c) X. Wang, Z. Cao, M. Zhang, L. Meng, Z. Ming, J. Liu, *Sci. Adv.* **2020**, *6*, eabb1952.
[25] Z. Jiang, B. Sun, Y. Wang, H. Gao, H. Ren, H. Zhang, T. Lu, X. Ren, W. Wei, X. Wang, L. Zhang, J. Li, D. Ding, J. F. Lovell, Y. Zhang, *Adv. Healthcare Mater.* **2021**, *10*, 2100356.
[26] J. Li, T. Wang, A. R. Kirtane, Y. Shi, A. Jones, Z. Moussa, A. Lopes, J. Collins, S. M. Tamang, K. Hess, *Sci. Transl. Med.* **2020**, *12*, eabc0441.
[27] a) A. Woting, M. Blaut, *Nutrients* **2018**, *10*, 685; b) V. Caride, E. Prokop, F. Troncale, W. Buddoura, K. Winchenbach, R. McCallum, *Gastroenterology* **1984**, *86*, 714.
[28] S. Spranger, D. Dai, B. Horton, T. F. Gajewski, *Cancer Cell* **2017**, *31*, 711.
[29] a) B. Li, G. Wang, K. Miao, A. Zhang, L. Sun, X. Yu, J. H. Lei, L. Xie, J. Yan, W. Li, *Nat. Commun.* **2023**, *14*, 2518; b) E. R. Pereira, D. Kedrin, G. Seano, O. Gautier, E. F. J. Meijer, D. Jones, S.-M. Chin, S. Kitahara, E. M. Bouta, J. Chang, E. Beech, H.-S. Jeong, M. C. Carroll, A. G. Taghian, T. P. Padera, *Science* **2018**, *359*, 1403.
[30] a) H.-Y. Feng, Y. Yuan, Y. Zhang, H.-J. Liu, X. Dong, S.-C. Yang, X.-L. Liu, X. Lai, M.-H. Zhu, J. Wang, *Nano-Micro Lett.* **2021**, *13*, 145; b) M. Brown, F. P. Assen, A. Leithner, J. Abe, H. Schachner, G. Asfour, Z. Bago-Horvath, J. V. Stein, P. Uhrin, M. Sixt, D. Kerjaschki, *Science* **2018**, *359*, 1408.
[31] a) P. Harter, J. Sehouli, D. Lorusso, A. Reuss, I. Vergote, C. Marth, J.-W. Kim, F. Raspagliesi, B. Lampe, G. Aletti, *N. Engl. J. Med.* **2019**, *380*, 822; b) E. Van Cutsem, X. Sagaert, B. Topal, K. Haustermans, H. Prenen, *Lancet* **2016**, *388*, 2654.
[32] a) A. M. Hafner, B. Corthésy, H. P. Merkle, *Adv. Drug Delivery Rev.* **2013**, *65*, 1386; b) I. Márquez-Rodas, F. Longo, M. E. Rodriguez-Ruiz, A. Calles, S. Ponce, M. Jove, B. Rubio-Viqueira, J. L. Perez-Gracia, A. Gómez-Rueda, S. López-Tarruella, *Sci. Transl. Med.* **2020**, *12*, eabb0391.
[33] a) D. Jones, Z. Wang, I. X. Chen, S. Zhang, R. Banerji, P.-J. Lei, H. Zhou, V. Xiao, C. Kwong, J. W. M. van Wijnbergen, *Nat. Biomed. Eng.* **2021**, *5*, 1426; b) J. Dubrot, F. V. Duraes, L. Potin, F. Capotosti, D. Brighouse, T. Suter, S. LeibundGut-Landmann, N. Garbi, W. Reith, M. A. Swartz, *J. Exp. Med.* **2014**, *211*, 1153.
[34] a) M. Lu, H. Xing, W. Shao, T. Zhang, M. Zhang, Y. Wang, F. Li, Y. Weng, A. Zheng, Y. Huang, X.-J. Liang, *Adv. Mater.* **2022**, *34*, 2204765; b) X. Wang, Y. Q. Liu, C. C. Xue, Y. Hu, Y. Y. Zhao, K. Y. Cai, M. H. Li, Z. Luo, *Nat. Commun.* **2022**, *13*, 5685.